Vertical Eddy Iron Fluxes Support Primary Production in the Open Southern Ocean

Leading author: Takaya Uchida (takaya.uchida@univ-grenoble-alpes.fr)

Vertical Eddy Iron Fluxes Support Primary Production in the Open Southern Ocean

Takaya Uchida[1], Dhruv Balwada[3], Ryan Abernathey[1,2], Galen McKinley[1,2], Shafer Smith[3] & Marina Lévy[4]

[1]*Department of Earth and Environmental Sciences, Columbia University in the City of New York*

[2]*Division of Ocean and Climate Physics, Lamont-Doherty Earth Observatory*

[3]*Center for Atmosphere Ocean Science, Courant Institute of Mathematical Sciences, New York University*

[4]*Laboratoire d'Océanographie et du Climat, Institut Pierre Simon-Laplace*

The primary productivity of the Southern Ocean ecosystem, and associated biological carbon pump, is limited by the availability of the micronutrient iron. Riverine sediments and atmospheric dust supply iron at the ocean margins, but in the vast open ocean, iron reaches phytoplankton primarily when iron-rich sub-surface waters enter the euphotic zone, linking vertical transport processes to ecosystem productivity. In addition to mixed-layer entrainment, recent studies in the North Atlantic and Southern Ocean suggest that eddy transport may be a highly effective pathway for nutrient transport. Here, high-resolution physical/biogeochemical simulations of an open-Southern-Ocean ecosystem forced with a realistic seasonal cycle reveal that primary production is sustained via iron supply across the mixed layer base primarily due to mesoscale and submesoscale turbulence (hereafter "(sub)mesoscale eddies"). As model resolution is increased from 20 km to 5 km to 2 km, vertical eddy iron flux

and phytoplankton biomass increase strongly, despite shoaling of the mixed layer. Diagnostics from eddy resolving runs show that the increase in primary production is supported by iron supply due to (sub)mesoscale isopycnal stirring. We also highlight that properly tuned eddy parametrizations in non-eddying runs can replicate this isopycnal flux and consequently the amount of biomass. One important consequence is that iron recycling is second-order importance in explaining sustained summertime productivity, as eddies continue to supply iron to the mixed layer throughout the year. Since eddy mixing rates are sensitive to wind forcing and large-scale hydrographic changes, these findings open a new mechanism for modulating the Southern Ocean biological pump on climate timescales.

Budgets of iron, the limiting nutrient in the Southern Ocean for primary production (1; 2; 3), estimated from ship-track observations have emphasized the importance of dust deposition, lateral transport and recycling of iron, concluding that contributions from upwelling are negligible (4). More recently, however, one-dimensional process studies have highlighted the importance of mixed-layer entrainment (5) and vertical diffusion of iron (6) in regions remote from dust sources. Due to the sparse spatial and temporal coverage of in-situ iron observations and the intermittent nature of iron supply and phytoplankton blooms, a basin-scale view has generally relied on global circulation models (GCMs; 8; 9) and data assimilation products (10). A GCM intercomparison study showed that, although the iron sources and biogeochemical parameters varied widely, the global-mean iron concentrations were largely in agreement, a consequence of model tuning towards this target (11). When compared against individual ocean transects, however, the GCMs showed a large inter-model disagreement. This spread was attributed to differences in how each

model represented the scavenging of iron. Due to computational constraints, eddy tracer transport in GCMs must be parametrized, also potentially causing uncertainty in the physical processes transporting iron (12) and resulting ecosystem.

In addition to vertical diapycnal mixing and large-scale circulation, mesoscale eddies (on scales of roughly 20 - 200 km and to first order geostrophically balanced) can make a major contribution to tracer transport (13; 14). In the Southern Ocean, upward vertical mesoscale eddy heat fluxes counteract the downward flux of heat due to Ekman pumping (15), and mesoscale eddies help regulate the subduction of anthropogenic carbon from the surface into the interior (12; 16). At even smaller scales where the geostrophic approximation breaks down, submesoscale turbulence (roughly 1 - 20 km and associated with Rossby and Richardson numbers on the order of unity) generates vigorous vertical velocities near the surface (17; 18). In the North Atlantic, submesoscale turbulence has been argued to drive significant transport of nutrients across the mixed-layer base, supporting ecosystem productivity (19). Do eddies play the same role with iron in the Southern Ocean?

To our knowledge, this question has only been investigated by examining Lagrangian particle trajectories from a high-resolution numerical simulation of the Kerguelen region. Calculating iron concentration in the reference frame of Lagrangian particles, Rosso (20; 21) argued that submesoscale iron fluxes could enhance primary productivity by a factor of two. While suggestive, their simulation technique did not implement a full ecosystem model, account for the strong seasonal cycle in both turbulence and biology, nor include fluxes from vertical mixing or mixed-layer

entrainment. The relative contribution of eddies to the open-Southern-Ocean primary productivity therefore warrants further investigation.

Here we take a different approach: we run a state-of-the-art numerical simulation at submesoscale permitting resolution in an idealized channel configuration and force the model with a realistic seasonal cycle. Due to the approximate zonal symmetry of the Antarctic Circumpolar Current, such configurations can capture the broad characteristics of Southern Ocean circulation, tracer transport and ventilation (22; 23). The reduced computational cost (compared to a global-scale simulation) enables our model to reach physical and biogeochemical equilibrium, and the simple geometry facilitates straightforward interpretation of the dynamics.

Submesoscale permitting simulation of the open Southern Ocean ecosystem

We use the Masachusetts Institute of Technology general circulation model (24) (MITgcm) with an embedded full ecosystem model (25; 26). The model configuration is identical to a companion paper (27) where we quantify the relative contribution of submesoscale and mesoscale dynamics on the total vertical iron transport. For completeness, details of the set up are also summarised in Text S1 (Supplementary Information). In this study, we focus on the biogeochemical effect of eddy iron transport on primary production and whether eddy parametrizations in non-eddying runs can replicate this unresolved flux. A snapshot of the phytoplankton biomass and iron field in the top 300 m on November 1 from the 2 km run, during the height of spring bloom, is shown in Fig. 1. The Rossby deformation radius at the center of the domain is 14 km, so the horizontal resolution

of 2 km allows us to observe the imprint of mesoscale coherent features (18), such as fronts and eddies, in both iron and phytoplankton.

To simulate the interaction of this region with the rest of the ocean, iron and other nutrients are relaxed to climatological observational profiles at the Northern boundary; in the rest of the domain their concentrations evolve freely based on the simulated circulation and ecosystem. In order to isolate the role of open-ocean transport processes, we do not supply aeolian dust input at the surface or glacial and bathymetric iron sources from the South. The annual-zonal-mean iron transect (Fig. 1**c**) shows enhanced iron concentrations at depth and strong depletion near the surface. A comparison with GEOTRACES iron profiles from the Southern Ocean (Fig. 1**d**) indicates that our simulation has a realistic ferrocline structure, in contrast with most of the global-scale GCM simulations (11). Deep iron concentrations of roughly 0.4 μmol Fe m^{-3} at 1000 m coincide with the observational mean in the ACC, while near-surface concentrations (0.05 μmol Fe m^{-3}) are lower than the observational range. This discrepancy is likely due to the lack of aeolian, glacial and bathymetric sources (28), uncertainty in the ecosystem model parameters (11), and potentially due to the lack of storms which have been argued to enhance diffusive entrainment of iron from the interior (29). As a result, iron is the limiting nutrient year round in our simulations, while in the real ACC, silicate limitation is also expected to control diatom growth and transition in phytoplankton community composition (8; 9). Consequently, primary production in our model is biased slightly low, particularly over the summer (Text S2, Figs. S1, S2). Dust supply maps indicate a supply of dissolved iron to the Southern Ocean on the order of O(1 μmol Fe m^{-2} yr^{-1}) assuming 10% of total aerosol iron is soluble (30). It is important to note that dust deposition is estimated to

account for only about 10% of the overall iron supply in the Southern Ocean, while internal transports make up the rest (31). Hence, although it would be possible to force our modelled surface iron concentrations to become closer to observations by adding dust, here we focus exclusively on internal transport mechanisms.

The Southern Ocean ecosystem is highly seasonal, with a strong spring bloom occurring between November and January (32; 33). Our model exhibits a strong seasonal cycle, as seen from Fig. 2, which illustrates the simulated climatological seasonal cycle of important physical and biological quantities, averaged over the center of the domain. Our simulations therefore provide a unique opportunity to investigate how seasonality in biological processes interacts with the seasonal cycle in physical transport processes and mixing-layer depth (MLD; definition in Methods section). There is a strong spring bloom, with the vertically integrated phytoplankton biomass ($\langle \mathrm{C_p} \rangle$; definition given in Methods section) peaking in early November, after the wintertime MLD has started to shoal (Fig. 2**a**), consistent with previous characterizations of the spring bloom in the ACC (33). To characterize the strength of (sub)mesoscale turbulence, we also show the root-mean square of vertical velocity ($\overline{w^2}^{1/2}$), which mirrors the MLD closely. This suggests that the vertical velocities are associated with mixed-layer instability (MLI), a type of surface-intensified baroclinic instability associated with submesoscales driven by available potential energy within the mixed layer (34), which is more active in winter with deep mixed layers. It is interesting to note that the vertical eddy iron flux ($w'\mathrm{Fe}'$; where $(\cdot)'$ is defined as the anomaly from the seasonal and zonal climatology using 15-daily snapshot outputs) is in phase with the biomass and not with vertical velocity itself (Fig. 2**a**). This suggests that energetic vertical velocities alone are not a

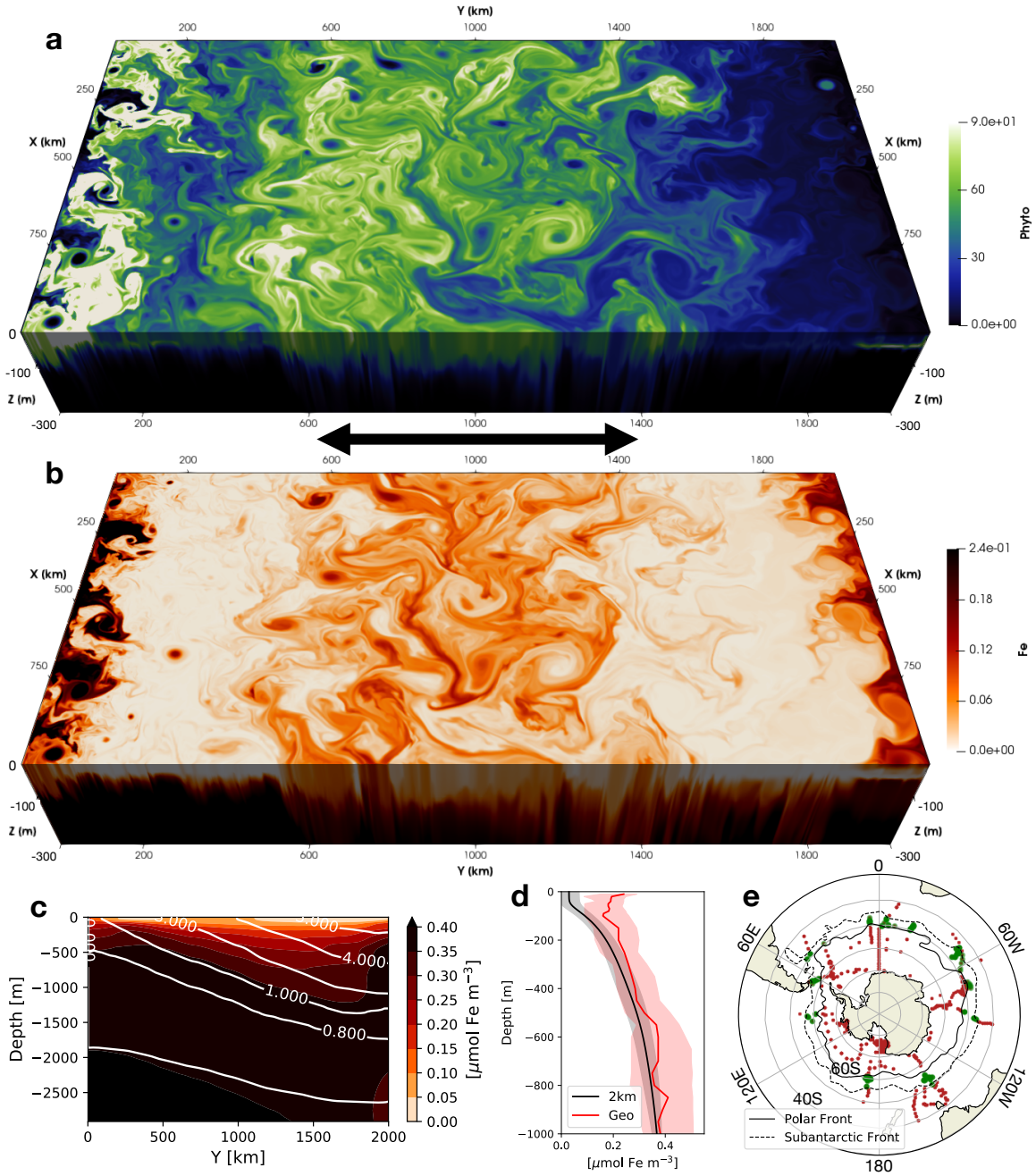

Figure 1: **A snapshot of phytoplankton biomass in (mg C m^{-3}) and iron in (μmol Fe m^{-3}) in the top 300 m; a,b. c** The zonal mean transect of iron and **d** vertical profile averaged over the meridional extent of $y = 600$ - 1400 km shown as the black arrow in **a** for our 2 km run (black) and median of the GEOTRACES dataset (red) acquired through personal communication with Tagliabue (6) over all profiles in the open ocean region between the climatological position of Polar and Subantarctic front (green; **e**) after applying a three-point median filter in the vertical. The frontal positions were taken from (7) and extended by 1° to the south and north respectively to incorporate more profiles. The colored shading show the standard deviation for the 2 km run and due to the lack of spatial coverage, the interquartile range is shown for GEOTRACES. The GEOTRACES dataset was biased towards austral summer so the data used in **d** for the 2 km run is over Nov.-Feb.

sufficient proxy for vertical tracer transport but need to correlate with tracer concentration.

The spring bloom is quantified via $\langle C_p \rangle$, which allows us to define the bloom *onset* ($\langle C_p \rangle$ minimum) and *apex* ($\langle C_p \rangle$ maximum) (Fig. 2**a**; (35)). The onset is in late July during the deepening of wintertime mixing layer, and the apex occurs in early November even though surface light conditions (γ^I; eqn. (S3)) continue to improve over the summer (November-January; Fig. 2**b**). The decrease in nutrient limitation factor (γ^N; eqn. (S4)), on the other hand, from 0.8 to 0.2 coincides with the apex and is in phase with iron concentration dropping from 0.13 to 0.03 μmol m^{-3} (Fig. 2**b**). (The limitation factors ("γ"s $= 0$ - 1) indicate ideal growth conditions when they are unity and zero for no-growth conditions. The effect of grazing by zooplankton is shown in Text S3, Fig. S3.) This indicates that the decline of the spring bloom in our simulation is due to iron limitation, and not associated with light conditions.

Vertical eddy and diffusive iron supply for primary production

To understand what controls the iron concentrations, we now examine the ecosystem in the time-depth plane. The top row of Fig. 3 shows horizontally averaged phytoplankton concentration and vertical iron fluxes by eddies and diffusion vs. time and depth over the seasonal cycle from the 2 km run. Iron concentration is given in Fig. 3**f** showing signals of wintertime entrainment with the orange contours dipping into the ML around September. (We show the complete zonal-mean iron budget in Fig. S1 and time-depth plots of biogeochemical iron consumption in Fig. S2.) As in Fig. 2**a**, there is a strong spring bloom and a mild autumn bloom. Some phytoplankton live

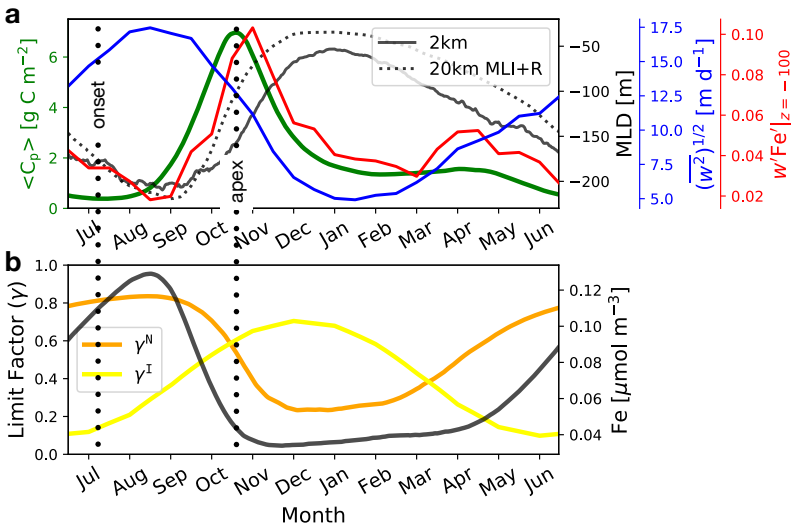

Figure 2: **Time series of the daily-mean vertically integrated phytoplankton biomass ($\langle \mathbf{C_p} \rangle$; green), daily mean of MLD for the 2 km (black solid) and 20 km MLI+R run (black dotted) averaged over the meridional extent of $y = 600$ - 1400 km; a.** The seasonal cycle of the root mean square of vertical velocity spatially averaged over the same meridional extent and over 100 m depth from the 2 km run ($\overline{w^2}^{1/2}$) is shown in blue, and spatially averaged vertical eddy iron flux ($w'\mathrm{Fe}'$ [μmol Fe m^{-2} d^{-1}]) at 100 m depth in red. **b** The spatial median over the top 100 m of growth rate limitation factors due to nutrient (γ^{N}; orange) and light (γ^{I}; yellow) where the former is due to iron year round in our simulation. The iron concentration (Fe) averaged over the top 100 m is plotted in black against the right axis.

below the ML base, particularly during summer when the ML is shallow. During wintertime (July-September) when the ML is deepening and light is low, there is low biomass but high iron concentration (Fig. 3**a**,**f**), consistent with the limitation factors ($\gamma^{\mathrm{I,N}}$, Fig. 2**b**).

Iron is supplied to the phytoplankton via three processes: recycling, entrainment and vertical mixing (here associated with the K-profile parametrization boundary layer; KPP (36)), and vertical eddy fluxes ($w'\mathrm{Fe}'$; explicitly resolved by the simulation). Figures 3**b**,**c** and S1 show how eddies and vertical (KPP) mixing work together to deliver iron to phytoplankton from depth. Vertical mixing is, by construction, only active within the ML. When vertical gradients of iron are actively sustained by biological consumption (e.g. during the bloom), vertical mixing drives a strong upward diffusive iron flux. This diffusive flux goes to zero at the ML base where KPP turns off. Eddy fluxes, in contrast, peak roughly at the ML base and extend deep into the iron-rich interior, with a magnitude comparable to the diffusive flux in the ML. Thus, eddies play a crucial role in bringing iron across the ML base, where it can be handed off to vertical mixing and delivered to near-surface phytoplankton.

Vertical eddy iron transport is absent from previous estimates of the Southern Ocean iron budget (4; 5; 6). One-dimensional iron budgets suggest that during summer, vertical mixing is not strong enough to supply the iron needed to sustain the observed productivity, implying strong iron recycling within the ecosystem (6). Our simulations challenge this conclusion, showing that vertical eddy transport can provide a year-round source of iron (Fig. 3**b**) which exceeds the magnitude of iron recycling (Fig. S1).

With the 2 km run as a reference, we use spatial resolution as a parameter to modulate the strength of eddy transport, running two other simulations at eddy-permitting resolutions of 5 km and 20 km. The basin-wide density and iron stratification for each resolution are given in Fig. S4. Figure 4 shows the annual median of vertically integrated phytoplankton biomass plotted against the annual mean of total (dominated by eddy) vertical iron flux across the ML base, or 100 m, whichever is deeper. This depth scale is chosen to exclude KPP mixing from the flux, and is roughly the depth phytoplankton cease to exist (Fig. 3**a**,**c**). As resolution increases from 20 km to 2 km for runs without any eddy parametrizations (red markers in Fig. 4), the annual median of daily averaged phytoplankton biomass ($\overline{\langle \mathrm{C_p} \rangle}$) nearly doubles from 0.67 to 1.45 g C m^{-2} in a roughly linear relationship with the annual-mean total (eddy+diffusive) iron transport (F^z_{Fe}), which increases from 7 to 27 μmol Fe m^{-2} yr^{-1}. This occurs despite a shoaling of the ML, which reduces the entrainment of iron. Thus, in our model ecosystem, eddies effectively control the primary productivity. We show the time-depth plot of vertical eddy iron flux from each run in Fig. S5.

[Sub]mesoscale eddy parametrizations

As we move to coarser resolution, we also ask whether conventional eddy parameterizations can provide the missing iron flux. We run three additional simulations at 100 km and 20 km resolution. The former represents a standard Coupled Model Intercomparison Project (CMIP)-class ocean GCM, while the latter the newer class of mesoscale-permitting GCMs (37). Due to limiting computational resources, we will continue to rely on non-eddying and mesoscale permitting GCMs for global climate and carbon cycle simulations. It is, therefore, informative to examine

how commonly employed parametrizations perform compared to submesoscale permitting simulations. The three different eddy parameterizations we experiment with are: Gent-McWilliams' eddy-induced velocity parametrization (GM; 38) in order to represent unresolved mesoscale restratification in the interior, isopycnal tracer diffusion (Redi; 39) to represent mesoscale stirring of tracers, and mixed-layer instability (MLI) parametrization (40) to represent the shoaling of ML due to otherwise resolved MLI. The runs are:

- `100 km GM+R` – with GM and Redi at 100 km resolution. We allowed the GM coefficient to vary between 200-2500 $m^2\ s^{-1}$, depending on the vertical-mean Richardson number (41), and chose a tapering scheme which accounted for a smooth transition between the diabatic boundary layer and adiabatic interior (42). The Redi diffusivity was chosen as 1000 $m^2\ s^{-1}$.
- `20 km MLI+R` – with MLI and Redi at 20 km resolution. We tuned the MLI parameters to produce the same wintertime MLD as the 2 km simulation (Fig. 2**a**, black dashed curve). The Redi diffusivity was chosen as 200 $m^2\ s^{-1}$, smaller than the case above with mesoscale eddies partially resolved at 20 km resolution.
- `20 km MLI` – with the MLI parametrization at 20 km resolution.

Further details on each configuration are given in Text S4.

The parameters in eddy parametrizations in global climate simulations are chosen operationally, without community-wide established best practices. In our study, we performed extensive experimentation with different combinations of eddy parameterizations and parameters, here re-

porting only the most relevant results. We discovered that, with a novel combination of choices, the parametrized eddy flux in 100 km GM+R run captures the amplitude and timing of cross-ML-base vertical eddy iron transport, particularly around November as seen in the 2 km run (Figs. 3**b**,**e**). The vertical flux in the 100 km GM+R is the sum of KPP mixing, GM advection and Redi diffusion. In other words, a direct comparison of vertical iron flux between the 100 km GM+R and 2 km run is Fig. 3**e** against the sum of **b** and **c**. Although not shown, the resolved eddy advection contribution is negligible at 100 km resolution and vertical mixing (KPP) is contained within the ML. The cross-ML-base iron transport in Fig. 3**e** is, therefore, predominantly due to isopycnal eddy stirring. Setting the Redi diffusivity to zero — equivalent to no mesoscale isopycnal stirring — in the 100-km run results in F^z_{Fe} decreasing by a factor of two and vertically integrated annual phytoplankton biomass by $\sim$40%. The pulse of iron coincides roughly with the spring bloom apex in early November in both the 2 km and 100 km GM+R runs, but summertime (January-March) biomass is higher within the top 100 m in the former (Fig. 3**a**,**d**). The higher summertime biomass in the 2 km run may be due to partially resolved MLI actively generating vertical iron gradients within the top 100 m, allowing for larger diffusive flux in the top 100 m for the 2 km run than in the 100 km GM+R run (Fig. 3**c**,**e**).

We plot phytoplankton biomass against vertical iron transport also for the parametrized runs in Fig. 4. Consistent with Fig. 3, they remain similar between the 2 km and 100 km GM+R runs (Fig. 4). The 20 km MLI+R comes close to the 5 km run (Fig. 4) with Redi diffusion adding cross-ML-base iron transport (Fig. S6). The MLI parametrization contribution, intended to replicate the restratification of the ML and not eddy tracer transport (40), is contained within the ML

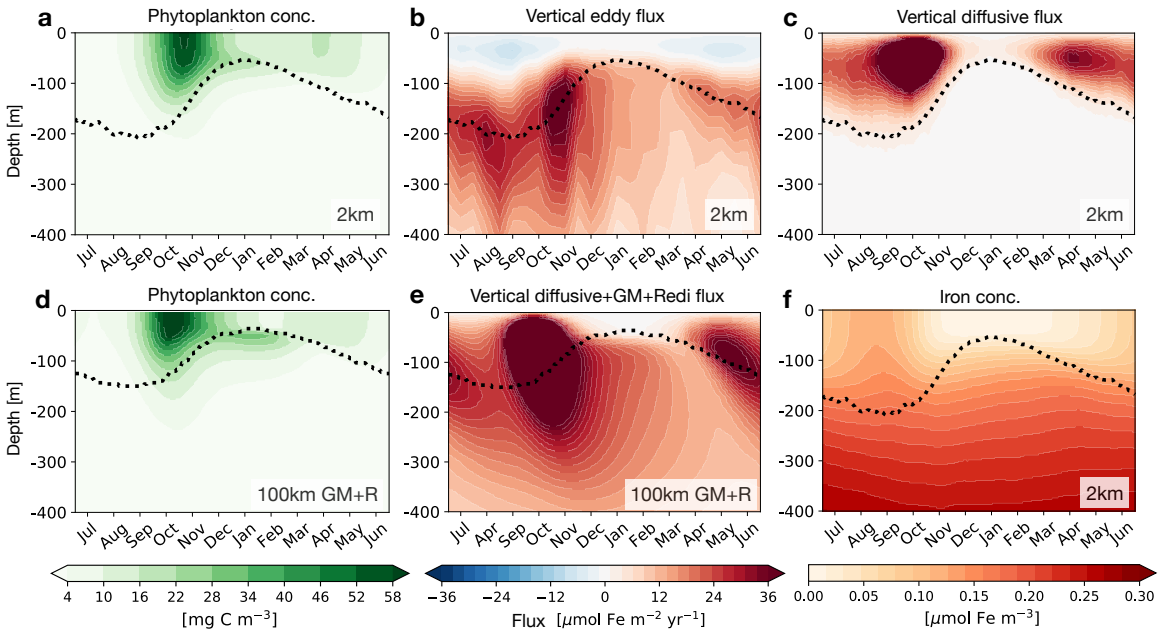

Figure 3: **Time-depth plots of the daily and spatial median of phytoplankton biomass; a. b,c** The spatial mean of vertical eddy transport using 15-daily snapshot outputs and diffusive iron transport using daily-averaged outputs. Panels **a**-**c**, and **f** (daily-averaged iron concentration) are from the 2 km run. **d,e** Daily-averaged phytoplankton biomass and the sum of vertical diffusive, GM and Redi iron flux from the 100 km GM+R run. The dotted lines in all panels show the mixing (mixed) layer depth for the 2 km (100 km GM+R) run. The *mixing*-layer depth (MLD) was too sensitive to the winds in the 100 km GM+R run, likely due to the GM tapering interacting with KPP (42). In all of our other runs, the *mixed*-layer depth defined as the depth at which the potential temperature decreased by 0.2°C from the surface (43) (not shown), proved to be very similar to the MLD so we used the mixed-layer depth for the 100 km GM+R run.

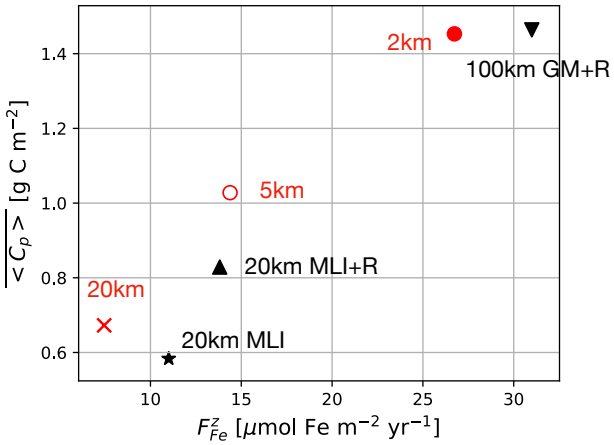

Figure 4: **The resolution dependence of annual median phytoplankton biomass ($\overline{\langle \mathbf{C_p} \rangle}$) on the annual mean of total vertical iron transport at the ML base or 100 m whichever is deeper ($F^z_{\mathbf{Fe}}$).** The runs without any eddy parametrizations are shown in red and the parametrized runs shown in black include the parametrized eddy flux.

and does not enhance cross-ML-base iron transport (Fig. S6**b**). Isopycnals, and consequently iron contours, in the interior at 20 km resolution are too steep compared to the 2 km run, with insufficient restratification relative to the resolved-mesoscale run (Figs. S4**c**, S7**b**). This results in weaker vertical gradients of iron and less net iron supply via entrainment and vertical eddy transport. The GM parametrization in the 100 km resolution run allows us to improve isopycnal steepness (Figs. S4**d**, S7**c**), and the Redi diffusivity is used to tune the isopycnal iron transport. The 20 km MLI run performs the worst amongst the parametrized runs (black markers in Fig. 4) with cross-ML-base eddy iron transport coming only from the resolved eddies at 20 km resolution.

Implications for iron budgets and biogeochemical modelling

We have shown, using a configuration representing the zonal-mean view of the Antarctic Circumpolar Current region, that eddy iron transport is crucial in supplying iron from depths across the

mixing-layer base (Figs. 3, 4). A study using a similar zonally re-entrant channel model, also found an increase in wintertime (August-October) vertical eddy iron transport, and consequently elevated primary production during September-October (29). Their spatial resolution of $1/24^{\circ}$, however, is similar to our 5 km run and the relative contribution of eddy transport in their study is likely underestimated (Fig. 4). Although 2 km resolution is state of the art for a basin-scale simulation coupled to a full biogeochemical model, it is not sufficient to fully resolve submesoscale processes including MLI (16). Based on the resolution dependence, we would expect the role of eddies in supplying iron to increase further with higher resolutions (44), but this would only strengthen the central finding that eddy iron transport modulates primary productivity in the open Southern Ocean.

Our results suggest that, in order to adequately capture the eddy iron transport, we should either at least partially resolve the submesoscales (2 km run) or completely parametrize the eddies using the *current generation* of GM (100 km GM+R run). In particular, we found that a novel combination of the Visbeck scheme for scaling the GM coefficient based on linear baroclinic instability (41), combined with the Ferrari tapering method (42), was uniquely able to mimic the eddy fluxes from the high-resolution run. Looking forward, it would be interesting to see whether *recently developed* energy backscattering GM parametrizations (45; 46) would improve tracer transport in mesoscale permitting models. The agreement of the 100 km GM+R run with the 2 km run, however, also highlights the potential significance of improving the parametrization for mesoscale isopycnal tracer (Redi) diffusion, which has been argued to be a significant factor in tracer ventilation using shiptrack observations in the Southern and Arctic Oceans (47). In our study, the Redi

diffusivity was tuned in an ad-hoc manner; future eddy parameterizations instead must be able to determine the correct value of this parameter based on physics in order to accurately simulate the response of the Southern Ocean biological pump to climate change. Considering that the MLI parametrization in its current formulation, intended for density restratification, does not capture eddy tracer transport (Fig. S6), it may also be beneficial to develop a new parametrization for the effects of submesoscale isopycnal tracer stirring.

There has been growing evidence regarding the relative importance of eddies in the biological carbon pump (48; 49; 50). The eddies responsible for supplying iron also export phytoplankton downwards in our simulation. We show in Fig. S8**a** the time-depth plot of vertical eddy phytoplankton transport ($w'C_p'$) for the 2 km run. The eddies subduct phytoplankton across the ML base and the magnitude increases with resolution (Fig. S8**b**). Nevertheless, the annual phytoplankton biomass and primary production increase with resolution (Figs. 4, S8**b**), indicating that the eddy supply of iron and resulting increase in productivity overcompensate for the loss of phytoplankton due to eddy subduction. Considering the annual maximum of eddy subduction occurs after the annual maximum in primary production, accurate representation of the magnitude and timing of eddy carbon subduction may be necessary to accurately model the Southern Ocean carbon cycle.

Methods

Mixing layer. The mixing-layer depth (MLD) is the boundary layer over which isotropic turbulent mixing, parameterized by the KPP in this simulation, is enhanced. Here, we quantify the depth of this highly variable layer as the zonal 99th percentile of the daily-averaged KPP boundary layer. In

our simulations, the *mixed*- and *mixing*-layer depth tended to be similar to each other. In general, however, the *mixed* layer often used in observational studies can be deeper than the *mixing* layer as the former is defined purely by thermal dynamical properties (43) while as latter is defined by kinematic properties. We argue that the *mixing* layer is the relevant depth scale for tracer transport as it is the layer over which diapycnal mixing is active (16). Figure 3**c** shows that diffusive fluxes are only active within the mixing layer in our simulation when eddies are explicitly resolved.

Integrated phytoplankton biomass. The integrated biomass ($\langle C_p \rangle$) is defined as the full-depth vertical integration of the spatial median ($y = 600$ - 1400 km, $x = 0$ - 1000 km) of C_p in order to incorporate phytoplankon existing below the mixing layer (5). We take the median as the phytoplankton biomass in our model approximately has a log-normal distribution.

References

1. Martin, John H and Gordon, Michael R and Fitzwater, Steve E. Iron in Antarctic waters. *Nature* **345**, 156 (1990).

2. De Baar, Hein JW and De Jong, Jeroen TM and Bakker, Dorothée CE and Löscher, Bettina M and Veth, Cornelis and Bathmann, Uli and Smetacek, Victor. Importance of iron for plankton blooms and carbon dioxide drawdown in the Southern Ocean. *Nature* **373**, 412 (1995).

3. Aumont, Oliver and Bopp, Laurent. Globalizing results from ocean in situ iron fertilization studies. *Global Biogeochemical Cycles* **20**, GB2017 (2006).

4. Bowie, Andrew R and Lannuzel, Delphine and Remenyi, Tomas A and Wagener, Thibaut

and Lam, Phoebe J and Boyd, Philip W and Guieu, Cécile and Townsend, Ashley T and Trull, Thomas W. Biogeochemical iron budgets of the Southern Ocean south of Australia: Decoupling of iron and nutrient cycles in the subantarctic zone by the summertime supply. *Global Biogeochemical Cycles* **23**, (2009).

5. Llort, Joan and Lévy, Marina and Sallée, Jean-Baptiste and Tagliabue, Alessandro. Onset, intensification, and decline of phytoplankton blooms in the Southern Ocean. *ICES Journal of Marine Science: Journal du Conseil* **72**, 1971–1984 (2015).

6. Tagliabue, Alessandro and Sallée, Jean-Baptiste and Bowie, Andrew R. and Lévy, Marina and Swart, Sebastiaan and Boyd, Philip W. Surface-water iron supplies in the Southern Ocean sustained by deep winter mixing. *Nature Geoscience* **7**, 314–320 (2014).

7. Orsi, Alejandro H and Whitworth III, Thomas and Nowlin Jr, Worth D. On the meridional extent and fronts of the Antarctic Circumpolar Current. *Deep Sea Research Part I: Oceanographic Research Papers* **42**, 641–673 (1995).

8. Moore, Keith J and Lindsay, Keith and Doney, Scott C and Long, Matthew C and Misumi, Kazuhiro. Marine ecosystem dynamics and biogeochemical cycling in the Community Earth System Model [CESM1 (BGC)]: Comparison of the 1990s with the 2090s under the RCP4. 5 and RCP8. 5 scenarios. *Journal of Climate* **26**, 9291–9312 (2013).

9. Moore, Mark C and Mills, Matthew M and Arrigo, Kevin R and Berman-Frank, Ilana and Bopp, Laurent and Boyd, Philip W and Galbraith, Eric D and Geider, Richard J and Guieu,

303 Cecile and Jaccard, Samuel L and others. Processes and patterns of oceanic nutrient limitation.
304 *Nature geoscience* **6**, 701–710 (2013).

305 10. Verdy, Ariane and Mazloff, Matthew R. A data assimilating model for estimating Southern
306 Ocean biogeochemistry. *Journal of Geophysical Research: Oceans* **122**, 6968–6988 (2017).

307 11. Tagliabue, Alessandro and Aumont, Olivier and DeAth, Ros and Dunne, John P and
308 Dutkiewicz, Stephanie and Galbraith, Eric and Misumi, Kazuhiro and Moore, Keith J and
309 Ridgwell, Andy and Sherman, Elliot and others. How well do global ocean biogeochemistry
310 models simulate dissolved iron distributions? *Global Biogeochemical Cycles* **30**, 149–174
311 (2016).

312 12. Gnanadesikan, Anand and Pradal, Marie-Aude and Abernathey, Ryan. Isopycnal mixing by
313 mesoscale eddies significantly impacts oceanic anthropogenic carbon uptake. *Geophysical Re-*
314 *search Letters* **42**, 4249–4255 (2015).

315 13. Wolfe, Christopher L and Cessi, Paola and McClean, Julie L and Maltrud, Mathew E. Vertical
316 heat transport in eddying ocean models. *Geophysical Research Letters* **35**, L23605 (2008).

317 14. Griffies, Stephen M and Winton, Michael and Anderson, Whit G and Benson, Rusty and
318 Delworth, Thomas L and Dufour, Carolina O and Dunne, John P and Goddard, Paul and
319 Morrison, Adele K and Rosati, Anthony and others. Impacts on ocean heat from transient
320 mesoscale eddies in a hierarchy of climate models. *Journal of Climate* **28**, 952–977 (2015).

321 15. Zika, Jan D and Le Sommer, Julien and Dufour, Carolina O and Molines, Jean-Marc and
322 Barnier, Bernard and Brasseur, Pierre and Dussin, Raphaël and Penduff, Thierry and Iudicone,

Daniele and Lenton, Andrew and others. Vertical eddy fluxes in the Southern Ocean. *Journal of Physical Oceanography* **43**, 941–955 (2013).

16. Balwada, Dhruv and Smith, Shafer K and Abernathey, Ryan. Submesoscale Vertical Velocities Enhance Tracer Subduction in an Idealized Antarctic Circumpolar Current. *Geophysical Research Letters* **45**, 9790–9802 (2018).

17. McWilliams, James C. Submesoscale currents in the ocean. *Proc. R. Soc. A* **472**, 20160117 (2016).

18. Lévy, Marina and Franks, Peter JS and Smith, Shafer K. The role of submesoscale currents in structuring marine ecosystems. *Nature communications* **9**, 4758 (2018).

19. Lévy, Marina and Ferrari, Raffaele and Franks, Peter JS and Martin, Adrian P and Rivière, Pascal. Bringing physics to life at the submesoscale. *Geophysical Research Letters* **39**, L14602 (2012).

20. Rosso, Isabella and Hogg, Andrew McC and Strutton, Peter G and Kiss, Andrew E and Matear, Richard and Klocker, Andreas and van Sebille, Erik. Vertical transport in the ocean due to submesoscale structures: Impacts in the Kerguelen region. *Ocean Modelling* **80**, 10–23 (2014).

21. Rosso, Isabella and Hogg, Andrew McC and Matear, Richard and Strutton, Peter G. Quantifying the influence of sub-mesoscale dynamics on the supply of iron to Southern Ocean phytoplankton blooms. *Deep Sea Research Part I: Oceanographic Research Papers* **115**, 199–209 (2016).

342 22. Abernathey, Ryan and Ferreira, David and Klocker, Andreas. Diagnostics of isopycnal mixing
343 in a circumpolar channel. *Ocean Modelling* **72**, 1–16 (2013).

344 23. Abernathey, Ryan and Ferreira, David. Southern Ocean isopycnal mixing and ventilation
345 changes driven by winds. *Geophysical Research Letters* **42**, 10–357 (2015).

346 24. Marshall, John and Adcroft, Alistair and Hill, Chris and Perelman, Lev and Heisey, Curt.
347 A finite-volume, incompressible Navier Stokes model for studies of the ocean on parallel
348 computers. *Journal of Geophysical Research: Oceans* **102**, 5753–5766 (1997).

349 25. Dutkiewicz, Stephanie and Follows, Michael J and Bragg, Jason G. Modeling the coupling of
350 ocean ecology and biogeochemistry. *Global Biogeochemical Cycles* **23**, GB4017 (2009).

351 26. Gloege, Lucas and McKinley, Galen A and Mouw, Colleen B and Ciochetto, Audrey B. Global
352 evaluation of particulate organic carbon flux parameterizations and implications for atmo-
353 spheric pCO2. *Global Biogeochemical Cycles* **31**, 1192–1215 (2017).

354 27. Uchida, Takaya and Balwada, Dhruv and Abernathey, Ryan and McKinley, Galen and Smith,
355 Shafer and Lévy, Marina. The contribution of submesoscale over mesoscale eddy iron trans-
356 port in the open Southern Ocean. *Journal of Advances in Modeling Earth Systems* (2019).
357 doi:10.1029/2019MS001805.

358 28. Boyd, Philip W and Ellwood, Michael J. The biogeochemical cycle of iron in the ocean. *Nature*
359 *Geoscience* **3**, 675–682 (2010).

360 29. Nicholson, Sarah A and Lévy, Marina and Jouanno, Julien and Capet, Xavier and Swart, Se-
361 bastiaan and Monteiro, Pedro MS. Iron supply pathways between the surface and subsurface

362 waters of the Southern Ocean: from winter entrainment to summer storms. *Geophysical Re-*
363 *search Letters* (2019). doi:10.1029/2019GL084657.

364 30. Duce, Robert A and Tindale, Neil W. Atmospheric transport of iron and its deposition in the
365 ocean. *Limnology and Oceanography* **36**, 1715–1726 (1991).

366 31. Sarmiento, Jorge L. *Ocean biogeochemical dynamics*. (Princeton University Press, 2013).

367 32. Sallée, Jean-Baptiste and Llort, J. and Tagliabue, A. and Lévy, M. Characterization of distinct
368 bloom phenology regimes in the Southern Ocean. *ICES Journal of Marine Science: Journal*
369 *du Conseil* **72**, 1985–1998 (2015).

370 33. Ardyna, Mathieu and Claustre, Hervé and Sallée, Jean-Baptiste and D'Ovidio, Francesco and
371 Gentili, Bernard and Van Dijken, Gert and D'Ortenzio, Fabrizio and Arrigo, Kevin R. Delin-
372 eating environmental control of phytoplankton biomass and phenology in the Southern Ocean.
373 *Geophysical Research Letters* **44**, 5016–5024 (2017).

374 34. Boccaletti, Giulio and Ferrari, Raffaele and Fox-Kemper, Baylor. Mixed layer instabilities and
375 restratification. *Journal of Physical Oceanography* **37**, 2228–2250 (2007).

376 35. Behrenfeld, Michael J and Boss, Emmanuel S. Student's tutorial on bloom hypotheses in the
377 context of phytoplankton annual cycles. *Global change biology* **24**, 55–77 (2018).

378 36. Large, William G and McWilliams, James C and Doney, Scott C. Oceanic vertical mixing: A
379 review and a model with a nonlocal boundary layer parameterization. *Reviews of Geophysics*,
380 **32**, 363–403 (1994).

37. Hallberg, Robert. Using a resolution function to regulate parameterizations of oceanic mesoscale eddy effects. *Ocean Modelling* **72**, 92–103 (2013).

38. Gent, Peter R and Mcwilliams, James C. Isopycnal mixing in ocean circulation models. *Journal of Physical Oceanography* **20**, 150–155 (1990).

39. Redi, Martha H. Oceanic isopycnal mixing by coordinate rotation. *Journal of Physical Oceanography* **12**, 1154–1158 (1982).

40. Fox-Kemper, Baylor and Danabasoglu, Gokhan and Ferrari, Raffaele and Griffies, Stephen M and Hallberg, Robert W and Holland, Marika M and Maltrud, Mathew E and Peacock, Synte and Samuels, Bonita L. Parameterization of mixed layer eddies. III: Implementation and impact in global ocean climate simulations. *Ocean Modelling* **39**, 61–78 (2011).

41. Visbeck, Martin and Marshall, John and Haine, Tom and Spall, Mike. Specification of eddy transfer coefficients in coarse-resolution ocean circulation models. *Journal of Physical Oceanography* **27**, 381–402 (1997).

42. Ferrari, Raffaele and McWilliams, James C and Canuto, Vittorio M and Dubovikov, Mikhail. Parameterization of eddy fluxes near oceanic boundaries. *Journal of Climate* **21**, 2770–2789 (2008).

43. de Boyer Montégut, Clément and Madec, Gurvan and Fischer, Albert S and Lazar, Alban and Iudicone, Daniele. Mixed layer depth over the global ocean: An examination of profile data and a profile-based climatology. *Journal of Geophysical Research: Oceans* **109**, C12003 (2004).

401 44. Bachman, Scott Daniel and Taylor, John R and Adams, Kate A and Hosegood, Phil J.
402 Mesoscale and submesoscale effects on mixed layer depth in the Southern Ocean. *Journal*
403 *of Physical Oceanography* **47**, 2173–2188 (2017).

404 45. Anstey, James A and Zanna, Laure. A deformation-based parametrization of ocean mesoscale
405 eddy Reynolds stresses. *Ocean Modelling* textbf112, 99–111 (2017).

406 46. Bachman, Scott D. The GM+ E closure: A framework for coupling backscatter with the Gent
407 and McWilliams parameterization. *Ocean Modelling* **136**, 85–106 (2019).

408 47. Naveira Garabato, Alberto C and MacGilchrist, Graeme A and Brown, Peter J and Evans, D
409 Gwyn and Meijers, Andrew JS and Zika, Jan D. High-latitude ocean ventilation and its role in
410 Earth's climate transitions. *Philosophical Transactions of the Royal Society A: Mathematical,*
411 *Physical and Engineering Sciences* **375**, 20160324 (2017).

412 48. Omand, Melissa M and D'Asaro, Eric A and Lee, Craig M and Perry, Mary Jane and Briggs,
413 Nathan and Cetinić, Ivona and Mahadevan, Amala. Eddy-driven subduction exports particulate
414 organic carbon from the spring bloom. *Science* **348**, 222–225 (2015).

415 49. Llort, Joan and Langlais, C and Matear, R and Moreau, S and Lenton, A and Strutton, Peter G.
416 Evaluating Southern Ocean Carbon Eddy-Pump From Biogeochemical-Argo Floats. *Journal*
417 *of Geophysical Research: Oceans* **123**, 971–984 (2018).

418 50. Resplandy, Laure and Lévy, Marina and McGillicuddy Jr, Dennis J. Effects of Eddy-Driven
419 Subduction on Ocean Biological Carbon Pump. *Global Biogeochemical Cycles* **33**, 1071–1084
420 (2019).

Acknowledgements This research was supported by NASA Award NNX16AJ35G as part of the SWOT Science Team. Abernathey acknowledges additional support from NSF Awards OCE-1553593 and OCE-1740648. Lévy acknowledges additional support from CNES and ANR award (ANR-16-CE01-0014). We thank the editor and two anonymous reviewers for their constructive comments on the manuscript.

Additional information Supplementary information is available in the online version of the paper.

Code availability The model configuration is available on Github (`doi:10.5281/zenodo.3266400`) and simulation outputs for 15-daily snapshot and monthly-averaged outputs of physical variables ($\mathbf{v}, \theta, \Phi$) are available on Pangeo (`doi:10.5281/zenodo.3358021`). Correspondence and requests for other variables and materials should be addressed to the leading author (email: takaya@ldeo.columbia.edu)

Competing interests The authors declare that they have no competing financial interests.